Computers and Fluids 213 (2020) 104755

Contents lists available at ScienceDirect

Computers and Fluids

journal homepage: www.elsevier.com/locate/compfluid

A novel Cahn–Hilliard–Navier–Stokes model with a nonstandard variable mobility for two-phase incompressible fluid flow

Junxiang Yang, Junseok Kim*

Department of Mathematics, Korea University, Seoul 02841, Republic of Korea

ARTICLE INFO

Article history:
Received 18 December 2019
Revised 1 September 2020
Accepted 10 September 2020
Available online 6 October 2020

Keywords:
Navier–Stokes equation
Nonstandard variable mobility
Cahn–Hilliard equation
Projection method

ABSTRACT

In this study, we present a novel Cahn–Hilliard–Navier–Stokes (CHNS) system with a nonstandard variable mobility for two-phase incompressible fluid flow. Unlike the classical constant mobility, the developed variable mobility has decreasing values nearby the interface and increasing values away from the interface, which minimizes the dynamics of the Cahn–Hilliard (CH) model nearby the interface. An unconditionally stable convex splitting method is used to solve the CH equation and the projection method is used to solve the NS equation. As benchmark tests, the Rayleigh–Taylor instability, drop deformation, and rising bubble are performed to show the accuracy and practicability of the proposed model. The computational results indicate that the proposed model accurately captures the interfacial position and keeps the interface region from being too much distorted.

1. Introduction

The phase-field method is an accurate and important approach in two-phase fluid flow simulations because the topology changes of interface can be easily captured by solving the phase-field equation without complex artificial works. The following Cahn–Hilliard–Navier–Stokes (CHNS) system is an extensively used phase-field model for two-phase incompressible fluid flows:

$$\phi_t + \nabla\cdot(\phi\mathbf{u}) = \frac{1}{Pe}\nabla\cdot(M\nabla\mu), \tag{1}$$

$$\mu = F'(\phi) - \epsilon^2\Delta\phi, \tag{2}$$

$$\rho(\phi)(\mathbf{u}_t + \mathbf{u}\cdot\nabla\mathbf{u}) = -\nabla p + \frac{1}{Re}\nabla\cdot\left(\eta(\phi)\left(\nabla\mathbf{u} + \nabla\mathbf{u}^T\right)\right) + \frac{\rho(\phi)}{Fr}\mathbf{g} + \mathbf{SF}, \tag{3}$$

$$\nabla\cdot\mathbf{u} = 0, \tag{4}$$

where $\phi = \phi(\mathbf{x}, t)$ and $\mu = \mu(\mathbf{x}, t)$ are the phase-field variable and chemical potential, respectively. Here, $\mathbf{x}$ and t are space and time variables. M is a general mobility, $F(\phi) = 0.25(1-\phi^2)^2$ is the double-well potential function, ϵ is a positive parameter related to the interfacial thickness, Pe is the Peclet number, $\mathbf{u}$ and p are the velocity and pressure fields, Re is the Reynolds number, Fr is the Froude number, and $\mathbf{g} = (0, -1)$ is the gravitational direction in two-dimensional space. One of the extensively used formula of continuous surface tension force is as follows [1]:

$$\mathbf{SF} = \frac{3\sqrt{2}\epsilon}{4We}\nabla\cdot\left(\frac{\nabla\phi}{|\nabla\phi|}\right)|\nabla\phi|\nabla\phi, \tag{5}$$

where We is the Weber number. Variable density and viscosity are

$$\rho(\phi) = \frac{\rho_1}{2}(1+\phi) + \frac{\rho_2}{2}(1-\phi) \text{ and}$$
$$\eta(\phi) = \frac{\eta_1}{2}(1+\phi) + \frac{\eta_2}{2}(1-\phi), \tag{6}$$

where ρ_1 and ρ_2 represent the densities of fluid 1 and fluid 2, respectively; η_1 and η_2 represent the viscosities of fluid 1 and fluid 2, respectively. The classical CHNS model (1)–(4) has been widely used in various two-phase incompressible fluid flow simulations, such as the Rayleigh–Taylor instability [2,3], Kelvin–Helmholtz instability [4], Rayleigh–Plateau instability [5], buoyancy-driven mixing [6], rising bubble [7,8], falling droplet [9], droplet deformation in shear flow [10–12], liquid jet formation [13,14], flow with surfactant [15,16], ferrofluid dynamics [17], and droplet impacting [18,19], etc. Because of the extensive applications of the CHNS model in science and engineering fields and the difficulties of finding analytical solutions, many researchers developed some accurate and efficient numerical schemes for the CHNS model in recent years.

* Corresponding author.
E-mail address: cfdkim@korea.ac.kr (J. Kim).
URL: http://math.korea.ac.kr/~cfdkim/ (J. Kim)

https://doi.org/10.1016/j.compfluid.2020.104755
0045-7930/

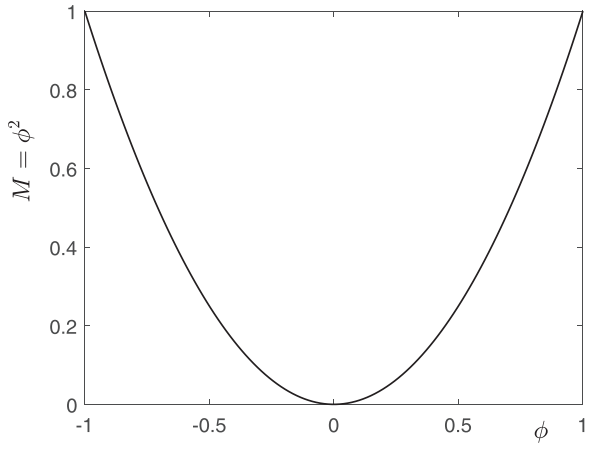

Fig. 1. Nonstandard mobility: $M = \phi^2$.

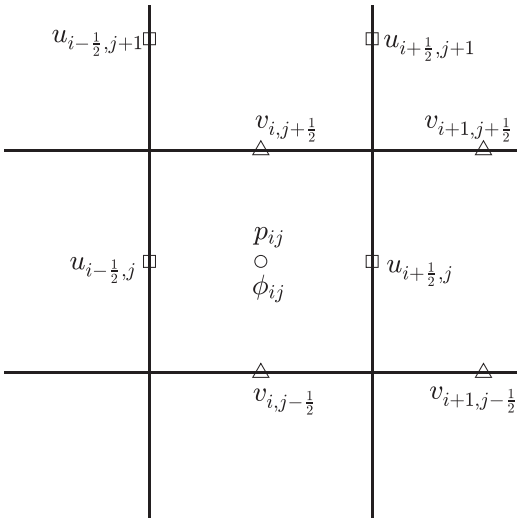

Fig. 2. Staggered marker-and-cell (MAC) spatial mesh.

Ding et al. [20] proposed a second-order time accurate numerical scheme for the classical CHNS system, where the CH equation was treated by using a two-step backward differentiation formula (BDF2) scheme, the viscosity term in NS equation was discretized by using the Crank–Nicolson (CN) scheme and the convection term was discretized by using the Adams–Bashforth (AB) scheme. Various numerical tests, such as the Rayleigh–Taylor instability and the rising bubble, were performed to show that their method is second-order accuracy in time and can be applied to two-phase flow problems with large density ratios. Shen and Yang [21] first developed a totally decoupled, unconditionally stable scheme for the CHNS model. Note that their scheme is efficient to implement because only elliptic equations are needed to solve in each time step. Chen and Shen [22] developed an efficient adaptive mesh and adaptive time method for solving the CHNS model. Zhu et al. [23] adopted the idea of recently developed scalar auxiliary variable (SAV) approach to propose an accurate energy stable scheme for the CHNS system. Wang et al. [24] studied a new stabilized phase-field method for two-phase flow problems with large density ratios and high Reynolds number. Moreover, the moving contact line problems for the CHNS model had been widely studied in Zhu et al. [15], Liu and Ding [18], Yu and Yang [25], especially for the solid-liquid interactions.

The CH model was originally proposed to model the spinodal decomposition in a binary mixture. Therefore, the interfacial length minimization is an intrinsic dynamics. In practice, we want to minimize this basic dynamics when the CH model is used for two-phase fluid flow simulations. To the best knowledge of authors, the constant mobility (i.e., $M = 1$) has been used in most two-phase flow simulations using the CHNS model. To minimize the intrinsic dynamics of the CH model, a natural approach is to choose a large Peclet number. However, a large Peclet number will make the interface region not be relaxed enough because the CH model is very sensitive to the Peclet number. In actual computation, an approximately uniform interface region is necessary to study the accurate evolution of interface, especially as the continuous surface tension force is considered.

The objective of this research is to propose a novel CHNS model with a nonstandard mobility, i.e., $M = \phi^2$ in Eq. (1), which is close to 1 in the bulk phase and decreases to 0 at the interface (see Fig. 1). The nonstandard mobility was used in the conservative Allen–Cahn equation [26], which has different dynamics from the CH equation. The proposed mobility minimizes the dynamics nearby the interface so that we do not need to choose a small Peclet number to make interface region to be uniform.

The rest of this article is organized as follows. In Section 2, we describe the numerical solution of the proposed model. In Section 3, various numerical experiments are performed. The conclusions are drawn in Section 4.

2. Numerical solution

We describe the numerical solution for Eqs. (1)–(4) with a nonstandard variable mobility: $M = \phi^2$. For simplicity, we present the two-dimensional case, the extension to three-dimensional space is straightforward. Let $\Omega = (a, b) \times (c, d)$ be the computational domain, which is discretized by using the uniform space step $h = (b-a)/N_x = (d-c)/N_y$, where N_x and N_y are the positive cell numbers along x- and y-directions, respectively. For $i = 1, 2, \ldots, N_x$ and $j = 1, 2, \ldots, N_y$, the cell centers are defined to be $(x_i, y_j) = (a + (i-0.5)h, c + (j-0.5)h)$. Let ϕ_{ij}^n, μ_{ij}^n, and p_{ij}^n be the approximations of $\phi(x_i, y_j, n\Delta t)$, $\mu(x_i, y_j, n\Delta t)$, and $p(x_i, y_j, n\Delta t)$, respectively. Here, $\Delta t = T/N_t$ is the time step, T and N_t are the total computational time and the number of temporal iterations, respectively. Let $u_{i+\frac{1}{2},j}^n$ and $v_{i,j+\frac{1}{2}}^n$ be the approximations of $u(x_{i+\frac{1}{2}}, y_j, n\Delta t)$ and $v(x_i, y_{j+\frac{1}{2}}, n\Delta t)$ at the cell edges. In this study, the staggered marker-and-cell (MAC) spatial mesh [27] is used, which means the phase-field variable: ϕ, chemical potential: μ, and pressure field: p are stored at the cell centers, the velocities: u and v are stored at the cell edges (see Fig. 2).

First, we numerically solve the NS Eqs. (3) and (4) by using the following projection method [28]: Using the given values $\mathbf{u}^n = (u^n, v^n)$ and ϕ^n, we calculate the intermediate velocity field $\tilde{\mathbf{u}}$ with the absence of pressure gradient:

$$\tilde{\mathbf{u}} = \mathbf{u}^n + \Delta t\left[\frac{1}{\rho(\phi^n)Re}\nabla_d \cdot \left(\eta(\phi^n)\left(\nabla_d \mathbf{u} + \nabla_d \mathbf{u}^T\right)^n\right) + \frac{\mathbf{SF}^n}{\rho(\phi^n)} - (\mathbf{u}\cdot\nabla_d\mathbf{u})^n + \frac{\mathbf{g}}{Fr}\right], \tag{7}$$

where the subscript d represents the discrete operator. The advection term is discretized by using the upwind scheme [28]. The spatial discretization of surface tension force $\mathbf{SF}$ can be found in Kim [1]. Then, we solve the following Eqs. (8) and (9) for the updated pressure filed: p^{n+1}:

$$\frac{\mathbf{u}^{n+1} - \tilde{\mathbf{u}}}{\Delta t} = -\frac{1}{\rho(\phi^n)}\nabla_d p^{n+1}, \tag{8}$$

$$\nabla_d \cdot \mathbf{u}^{n+1} = 0. \tag{9}$$

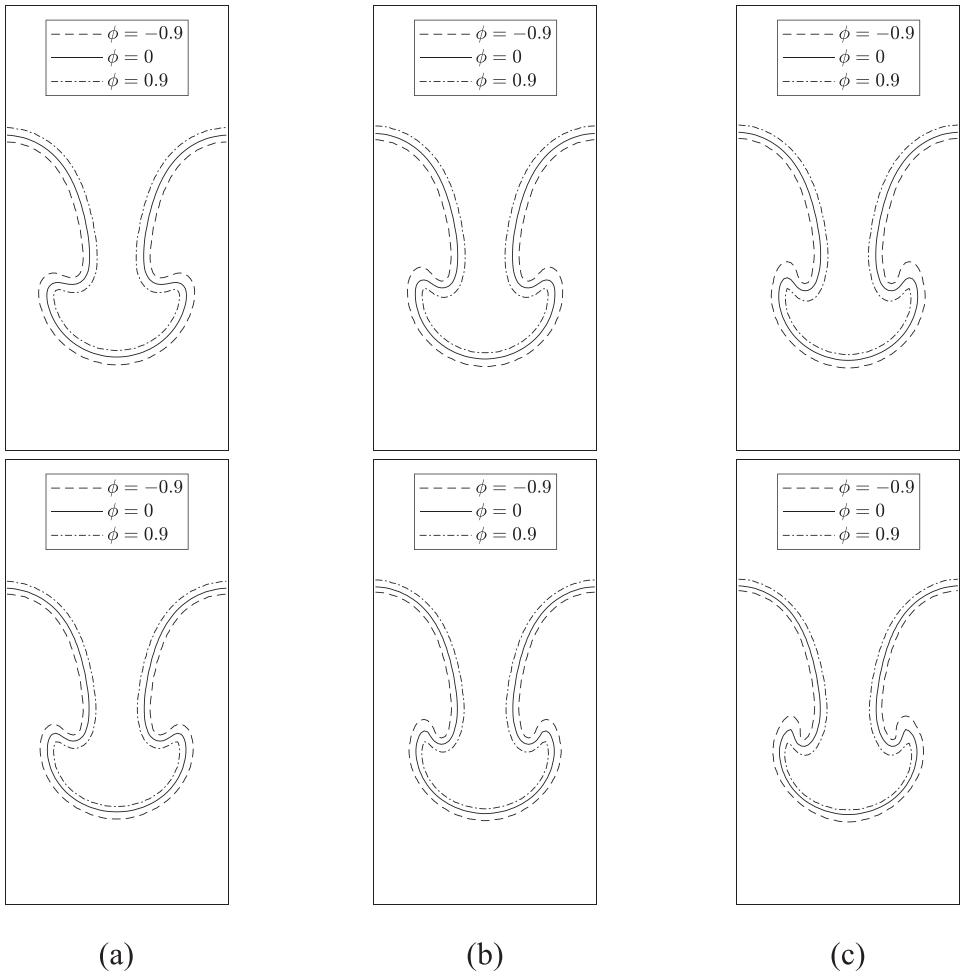

Fig. 3. Interface region ($\phi = -0.9, 0, 0.9$) for the constant mobility: $M = 1$ (first row) and the variable mobility: $M = \phi^2$ (second row) at $t = 2.125$. Here, (a), (b), and (c) represent the results for $Pe = 0.5/\epsilon$, $1/\epsilon$, and $2/\epsilon$, respectively.

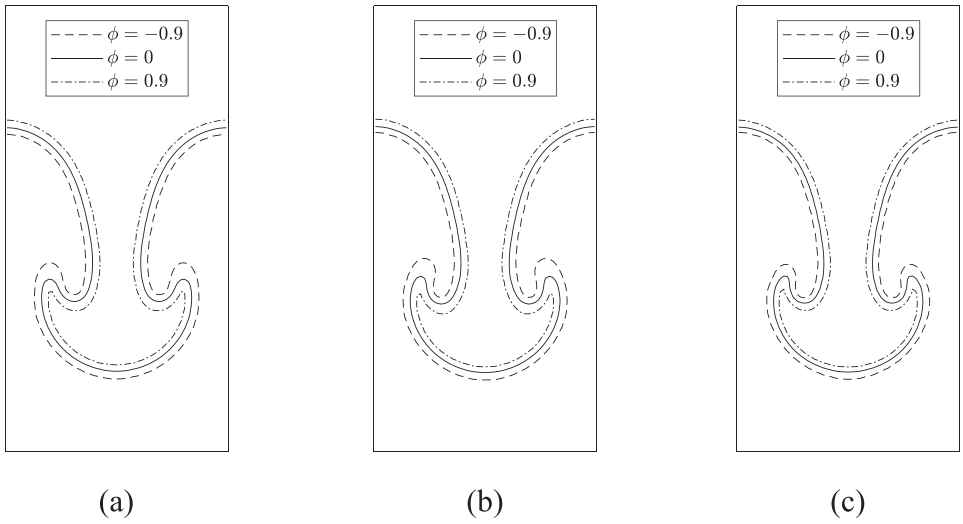

Fig. 4. Interface region ($\phi = -0.9, 0, 0.9$) at $t = 2.2725$ for the model with $M = 1$ and $Pe = 1/\epsilon$ (a), the model with $M = 1$ and $Pe = 2/\epsilon$ (b), and the model with $M = \phi^2$ and $Pe = 1/\epsilon$ (c).

By takeing the discrete divergence operation to Eq. (8) and using Eq. (9), we can obtain the pressure Poisson equation:

$$\nabla_d \cdot \left(\frac{1}{\rho(\phi^n)} \nabla_d p^{n+1} \right) = \frac{1}{\Delta t} \nabla_d \cdot \tilde{\mathbf{u}}. \tag{10}$$

Here, the multigrid method [29] is used to solve the linear system of Eq. (10). Thus, the updated velocity field can be obtained by:

$$\mathbf{u}^{n+1} = \tilde{\mathbf{u}} - \frac{\Delta t}{\rho(\phi^n)} \nabla_d p^{n+1}. \tag{11}$$

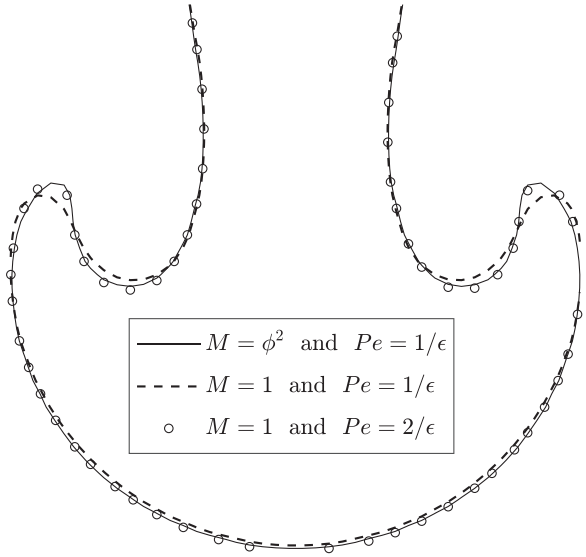

Fig. 5. Interfacial positions ($\phi = 0$) at $t = 2.2725$.

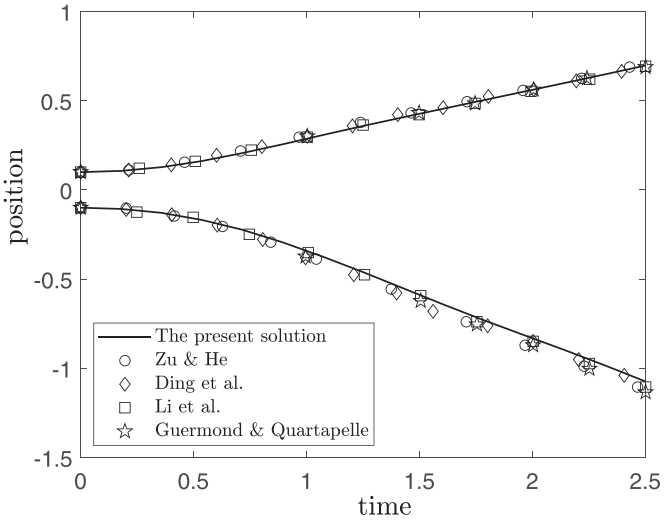

Fig. 7. Temporal evolutions of the normalized positions of rising bubble and falling spike.

Next, we use the unconditionally stable convex splitting method [30] to solve Eqs. (1) and (2), the discretizations are written to be

$$\frac{\phi_{ij}^{n+1} - \phi_{ij}^{n}}{\Delta t} = \frac{1}{Pe}\nabla_d \cdot \left(M_{ij}^{n}\nabla_d \mu_{ij}^{n+1}\right) - \nabla_d \cdot (\phi \mathbf{u})_{ij}^{n}, \tag{12}$$

$$\mu_{ij}^{n+1} = (\phi_{ij}^{n})^3 - \phi_{ij}^{n} + \epsilon^2 \Delta_d \phi_{ij}^{n+1}, \tag{13}$$

where $M_{ij}^{n} = (\phi_{ij}^{n})^2$. A nonlinear multigrid method [29] with Gauss–Seidel-type iteration is used to solve Eqs. (12) and (13). For more details of nonlinear multigrid method, see [29,31]. Here, the classical five-point discretization of Laplacian operator is used, i.e., $\Delta_d \phi_{ij} = \left(\phi_{i+1,j} + \phi_{i-1,j} + \phi_{i,j+1} + \phi_{i,j-1} - 4\phi_{ij}\right)/h^2$. The mass conservation is an important issue for two-phase flow simulation. Therefore, the following conservative discretization of the convec-

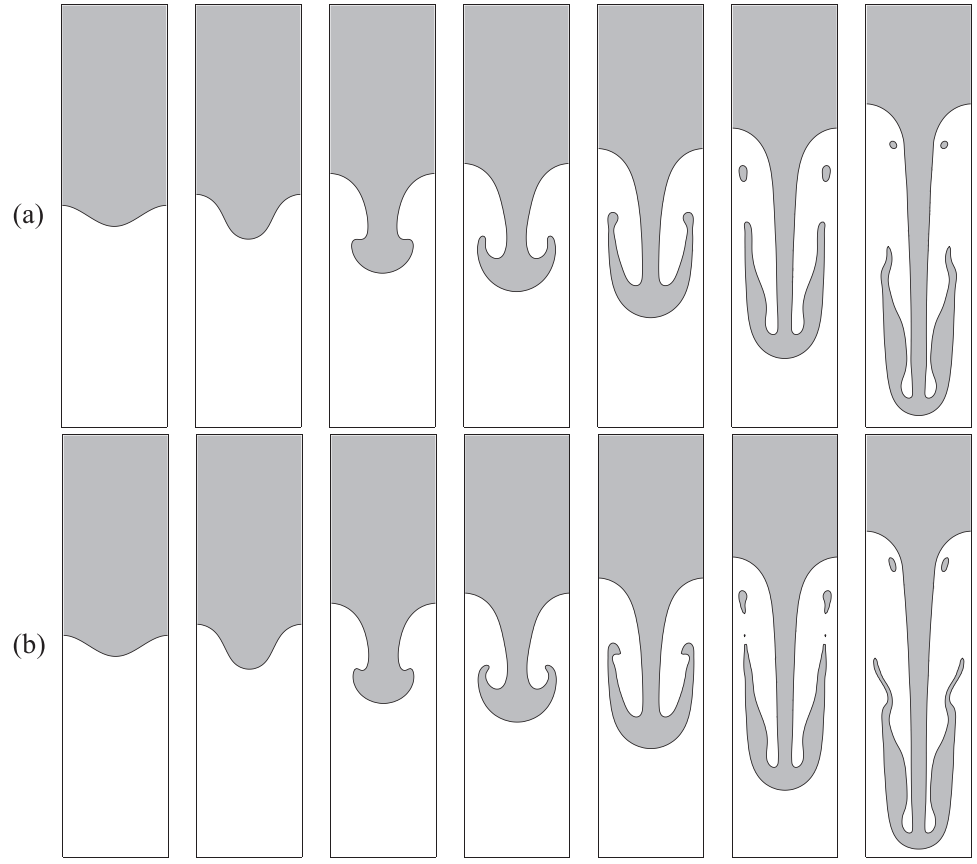

Fig. 6. Temporal evolutions of RTI for the classical model with $M = 1$ and $Pe = 1/\epsilon$ (a) and the proposed model with $M = \phi^2$ and $Pe = 1/\epsilon$ (b). The snapshots from the left to right in each row are: $t = 0,\ 1.01,\ 2.02,\ 2.525,\ 3.2825,\ 4.2925$, and 5.3025.

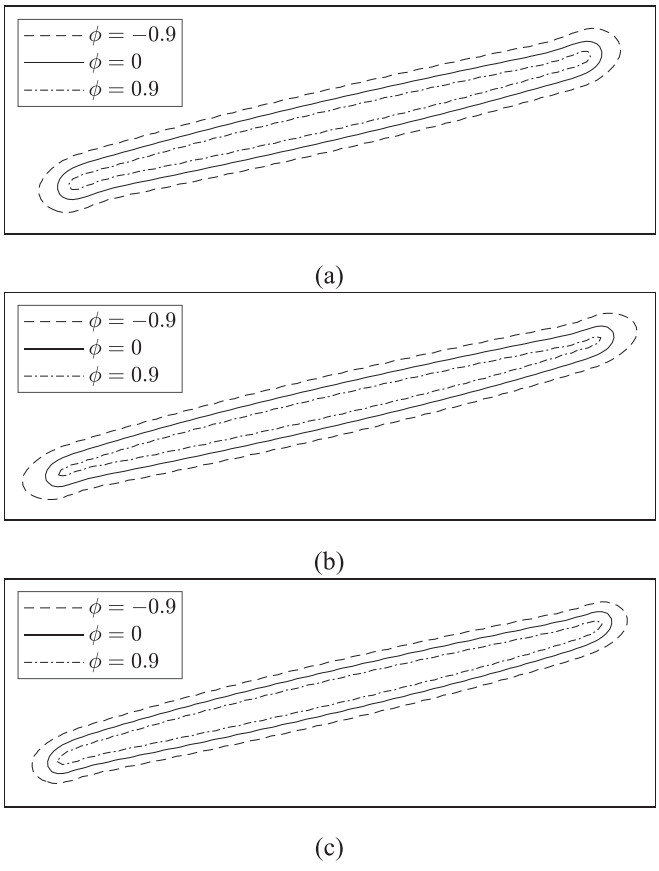

Fig. 8. Interface region ($\phi = -0.9, 0, 0.9$) at $t = 2$ for the model with $M = 1$ and $Pe = 1/\epsilon$ (a), the model with $M = 1$ and $Pe = 2/\epsilon$ (b), and the model with $M = \phi^2$ and $Pe = 1/\epsilon$ (c).

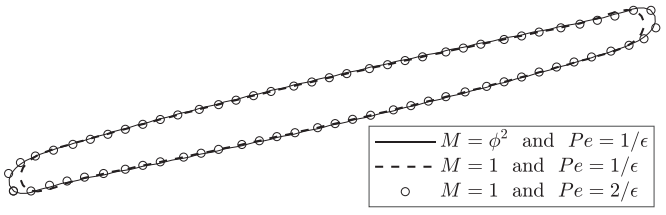

Fig. 9. Interfacial positions ($\phi = 0$) at $t = 2$ in shear flow.

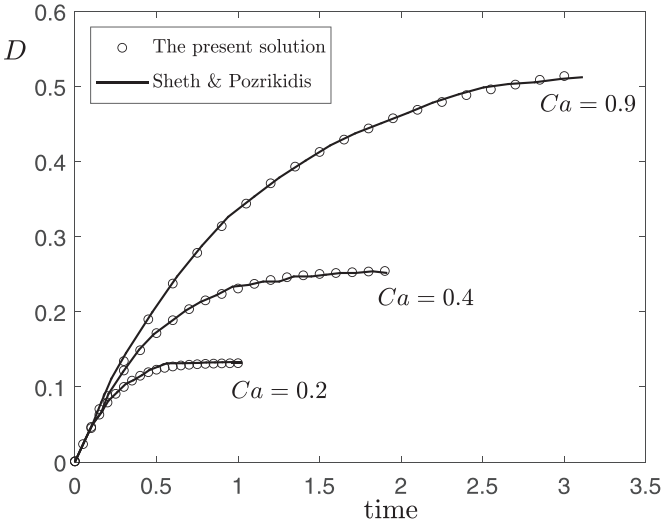

Fig. 10. Temporal evolutions of deformation parameter D for $Re = 1$, and $Ca = 0.2, 0.4, 0.9$.

tion term in Eq. (12) is used:

$$\nabla_d \cdot (\phi \mathbf{u})_{ij}^n = \frac{\left(\phi_{i+1,j}^n + \phi_{ij}^n\right) u_{i+\frac{1}{2},j}^n - \left(\phi_{ij}^n + \phi_{i-1,j}^n\right) u_{i-\frac{1}{2},j}^n}{2h} + \frac{\left(\phi_{i,j+1}^n + \phi_{ij}^n\right) v_{i,j+\frac{1}{2}}^n - \left(\phi_{ij}^n + \phi_{i,j-1}^n\right) v_{i,j-\frac{1}{2}}^n}{2h}. \quad (14)$$

Thus, we complete the numerical solution in one time cycle.

3. Numerical experiments

For the parameter ϵ, we use the formulation: $\epsilon_m = mh/[\sqrt{2}\tanh^{-1}(0.9)]$, which indicates that the interface region occupies approximately m grid points [32]. Unless otherwise specified, we use $\epsilon = \epsilon_4$. The viscosity-matched condition, i.e., $\eta_1 = \eta_2 = 1$, is considered in the following numerical tests.

3.1. Effect of Peclet (Pe) number

We investigate the effect of Pe number on the evolution of interface. The dynamics of the CH model is sensitive for the Pe number in the simulation. As reported in the previous studies [28], a small Pe number delays the evolution of interface, while a large Pe number makes the interface region not to be relaxed. Therefore, using a proper Pe is important in the simulation. Here, we consider the evolution of Rayleigh–Taylor instability (RTI) with constant mobility $M = 1$ and variable mobility $M = \phi^2$ in the domain $\Omega = (0, 1) \times (0, 2)$. The initial conditions are defined to be

$$\phi(x, y, 0) = \tanh\left(\frac{y - 1 - 0.1\cos(2\pi x)}{\sqrt{2}\epsilon}\right), \quad (15)$$

$$u(x, y, 0) = v(x, y, 0) = 0. \quad (16)$$

The following numerical parameters are used: $h = 1/64$, $\Delta t = 0.0025$, $Re = 3000$, and $Fr = 1$. The density ratio of fluid 1 and fluid 2 is $\rho_1 : \rho_2 = 3 : 1$. The surface tension is ignored, i.e., $We = \infty$. The results at $t = 2.125$ are illustrated in Fig. 3, where the first row and second row represent the results for $M = 1$ and $M = \phi^2$, respectively. Three columns (a), (b), and (c) are the results for $Pe = 0.5/\epsilon$, $1/\epsilon$, and $2/\epsilon$, respectively. As we can observe, a larger Pe number makes the interface region, i.e., $\phi = -0.9 \sim 0.9$, to be not uniform, while a smaller Pe number delays the evolution because of the dominating dynamics of the CH model. Therefore, $Pe = 1/\epsilon$ is a proper choice for both $M = 1$ and $M = \phi^2$. In the following tests, we will use $Pe = 1/\epsilon$ unless otherwise stated.

3.2. Two-dimensional RTI

First, the two-dimensional RTI is considered to compare the different dynamics of the models with constant mobility, $M = 1$ and variable mobility, $M = \phi^2$. We use the following initial conditions in the domain $\Omega = (0, 1) \times (0, 4)$:

$$\phi(x, y, 0) = \tanh\left(\frac{y - 2 - 0.1\cos(2\pi x)}{\sqrt{2}\epsilon}\right), \quad (17)$$

$$u(x, y, 0) = v(x, y, 0) = 0. \quad (18)$$

The numerical parameters keep the same as those in Section 3.1. For the model with variable mobility: $M = \phi^2$, the Pe number: $1/\epsilon$ is used. For the model with constant mobility $M = 1$, two different Pe numbers: $1/\epsilon$ and $2/\epsilon$ are considered. Fig. 4(a)–(c) illustrate the interface region ($\phi = -0.9 \sim 0.9$) at $t = 2.2725$ for the model with $M = 1$ and $Pe = 1/\epsilon$, the model with $M = 1$ and $Pe = 2/\epsilon$, and the model with $M = \phi^2$ and $Pe = 1/\epsilon$, respectively. The interfacial positions ($\phi = 0$) at $t = 2.2725$ are shown in Fig. 5. For the same Pe

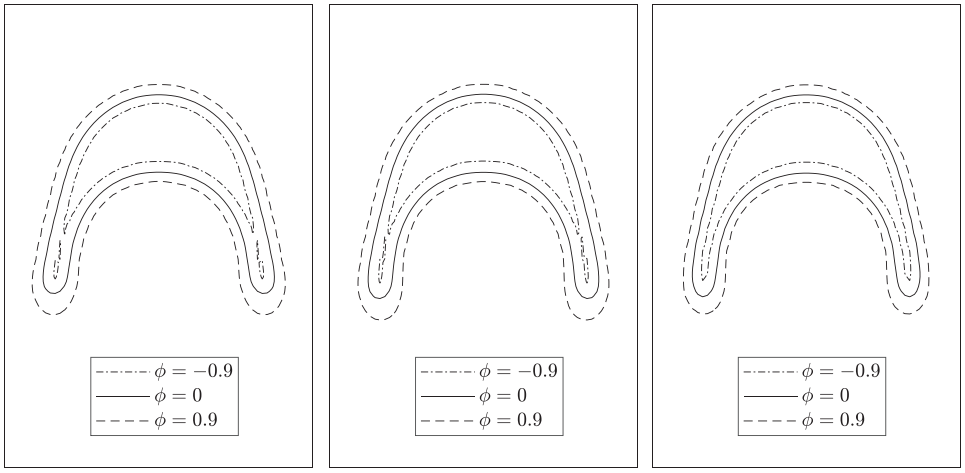

Fig. 11. Interface region ($\phi = -0.9, 0, 0.9$) at $t = 2$ for the model with $M = 1$ and $Pe = 1/\epsilon$ (a), the model with $M = 1$ and $Pe = 2/\epsilon$ (b), and the model with $M = \phi^2$ and $Pe = 1/\epsilon$ (c).

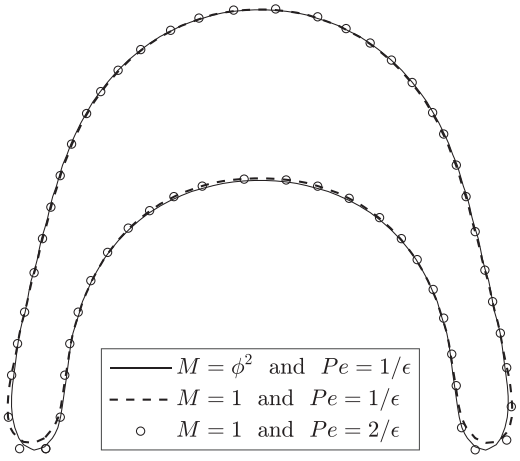

Fig. 12. Interfacial positions ($\phi = 0$) at $t = 1.7$ of the rising bubble.

number: $1/\epsilon$, the model with variable mobility minimizes the effect of the CH dynamics and captures a more accurate interfacial position than the model with constant mobility. By taking a larger Pe number: $2/\epsilon$, although the model with constant mobility can capture a more accurate interfacial position, the interface region is not uniform. We can confirm that the proposed model can accurately capture the interfacial position without using a larger Pe number and the interface region is approximately uniform.

To compare the dynamics of the classical model: $M = 1$ and $Pe = 1/\epsilon$ and the proposed model: $M = \phi^2$ and $Pe = 1/\epsilon$. The temporal evolutions of RTI are illustrated in Fig. 6(a) and (b), we can find that the proposed model captures more details during the interface evolution.

Then, we verify the solution of the proposed model by comparison with previous works performed by Zu and He [33], Ding et al. [20], Li et al. [34], and Guermond and Quartapelle [35]. The parameters are kept unchanged and the computation stops at $\tilde{t} = 2.5$ which is related to ours by the time scale: $\tilde{t} = t\sqrt{At}$, where $At = (\rho_1 - \rho_2)/(\rho_1 + \rho_2) = 0.5$ is the Atwood number. Fig. 7 shows the temporal evolutions of normalized positions of rising bubble and falling spike, we can find that our solution and previous results are in good agreement.

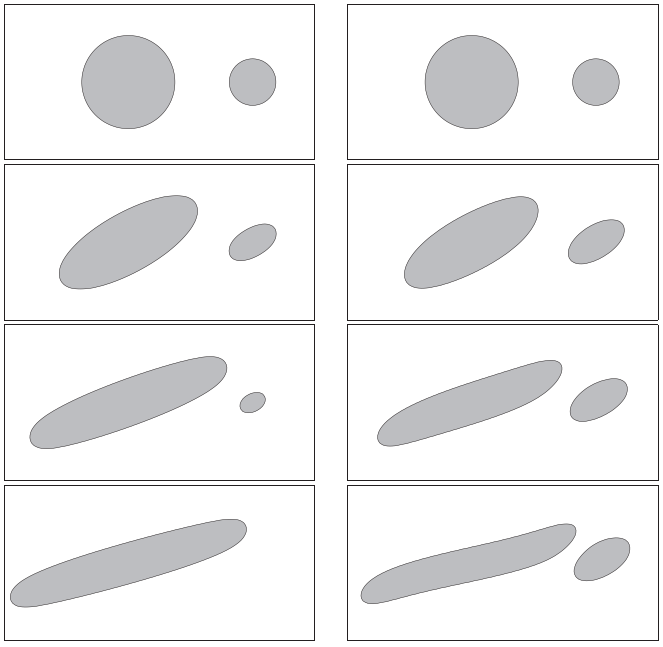

Fig. 13. Temporal evolutions of two droplets under shear flow by (a) the CACNS model and (b) the proposed model. The snapshots from the top to bottom are: $t = 0,\ 0.625,\ 1.25,$ and 1.75.

3.3. Two-dimensional drop deformation

Next, we compare the classical models: $M = 1$ and $Pe = 1/\epsilon$; $M = 1$ and $Pe = 2/\epsilon$ and the proposed model: $M = \phi^2$ and $Pe = 1/\epsilon$ by simulating the droplet deformation in shear flow. The initial conditions are defined as:

$$\phi(x, y, 0) = \tanh\left(\frac{0.25 - \sqrt{(x-1)^2 + (y-0.5)^2}}{\sqrt{2}\epsilon}\right), \tag{19}$$

$$u(x, y, 0) = 2y - 1, \quad v(x, y, 0) = 0 \tag{20}$$

in the domain $\Omega = (0, 2) \times (0, 1)$. To achieve the large deformation in the shear flow, a larger Weber number: $We = 100$ is used.

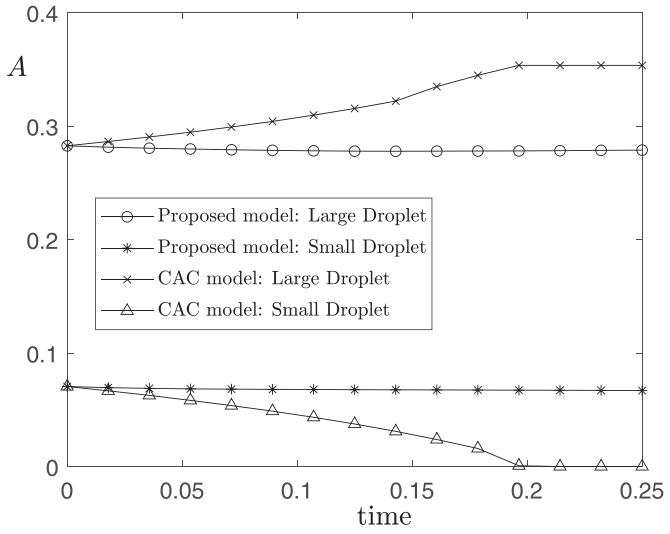

Fig. 14. Temporal evolution of local mass A enclosed by interface of each droplet.

Other numerical parameters are: $h = 1/64$, $\Delta t = 2h^2$, $Re = 10$, and $\rho_1 : \rho_2 = 1 : 1$. Fig. 8(a)–(c) illustrate the interface region ($\phi = -0.9 \sim 0.9$) at $t = 2$ for the model with $M = 1$ and $Pe = 1/\epsilon$, the model with $M = 1$ and $Pe = 2/\epsilon$, and the model with $M = \phi^2$ and $Pe = 1/\epsilon$, respectively. The interfacial positions ($\phi = 0$) at $t = 2$ are shown in Fig. 9. For the same Pe number: $1/\epsilon$, we can find that the model with variable mobility captures a more accurate interfacial position than the model with constant mobility. Although the model with constant mobility can capture a more accurate interfacial position by using $Pe = 2/\epsilon$, the interface region is not uniform. In the shear flow, the proposed model can still accurately capture the interfacial position under the large deformation. Moreover, The interface region can be approximately uniform at most when the proposed model is used.

The droplet deformation in shear flow is an important benchmark problem to verify the accuracy of surface tension. The continuous surface tension model in phase-field method requires an approximately uniform interface region to have an accurate computation. Thus, we verify the solution of the proposed model in shear flow by comparison with previous work performed by Sheth and Pozrikidis [36]. The initial conditions are set to be

$$\phi(x, y, 0) = \tanh\left(\frac{0.5 - \sqrt{(x-1)^2 + (y-1)^2}}{\sqrt{2}\epsilon}\right), \tag{21}$$

$$u(x, y, 0) = y, \quad v(x, y, 0) = 0 \tag{22}$$

in the domain $\Omega = (0, 2) \times (0, 2)$. The parameters are: $h = 1/32$, $\Delta t = 0.2h^2$, $Re = 1$, and $Pe = 1/\epsilon$. Three different Capillary numbers: $Ca = We/Re = 0.2$, 0.4, and 0.9 are considered. Fig. 10 is the time evolutions of deformation parameter, D. We can find that our solution and previous results are in good agreement.

3.4. Two-dimensional rising bubble

Then, we compare the classical models: $M = 1$ and $Pe = 1/\epsilon$; $M = 1$ and $Pe = 2/\epsilon$ and the proposed model: $M = \phi^2$ and $Pe = 1/\epsilon$ by simulating the rising bubble in ambient liquid with the following initial conditions:

$$\phi(x, y, 0) = \tanh\left(\frac{\sqrt{(x-1)^2 + (y-1)^2} - 0.5}{\sqrt{2}\epsilon}\right), \tag{23}$$

$$u(x, y, 0) = v(x, y, 0) = 0. \tag{24}$$

in the domain $\Omega = (0, 4) \times (0, 2)$. In this test, we use $h = 1/32$, $\Delta t = 0.2h^2$, $Re = 35$, $We = 125$, $Fr = 1$, and $\rho_1 : \rho_2 = 20 : 1$, where ρ_1 and ρ_2 are the densities of ambient liquid and light bubble, respectively. Fig. 11(a)–(c) illustrate the interface region ($\phi = -0.9 \sim 0.9$) at $t = 1.7$ for the model with $M = 1$ and $Pe = 1/\epsilon$, the model with $M = 1$ and $Pe = 2/\epsilon$, and the model with $M = \phi^2$ and $Pe = 1/\epsilon$, respectively. The interfacial positions ($\phi = 0$) at $t = 1.7$ are shown in Fig. 12. Comparing with the classical model, we can observe that the proposed model can accurately capture the interfacial position of rising bubble.

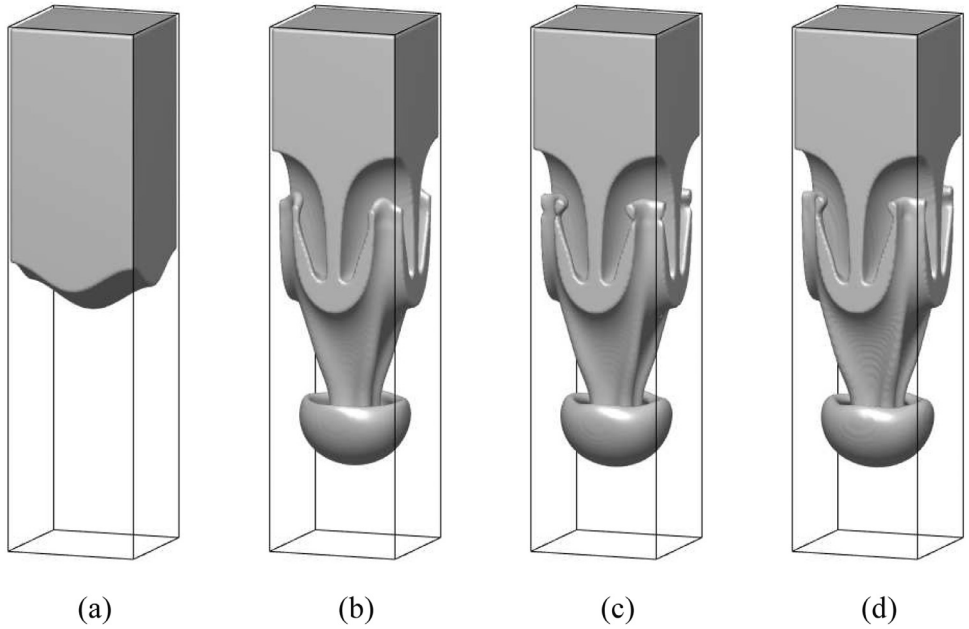

Fig. 15. (a) Initial state. Evolutions of interface ($\phi = 0$) at $t = 3$: (b) $M = 1$ and $Pe = 1/\epsilon$, (c) $M = 1$ and $Pe = 2/\epsilon$, (d) $M = \phi^2$ and $Pe = 1/\epsilon$.

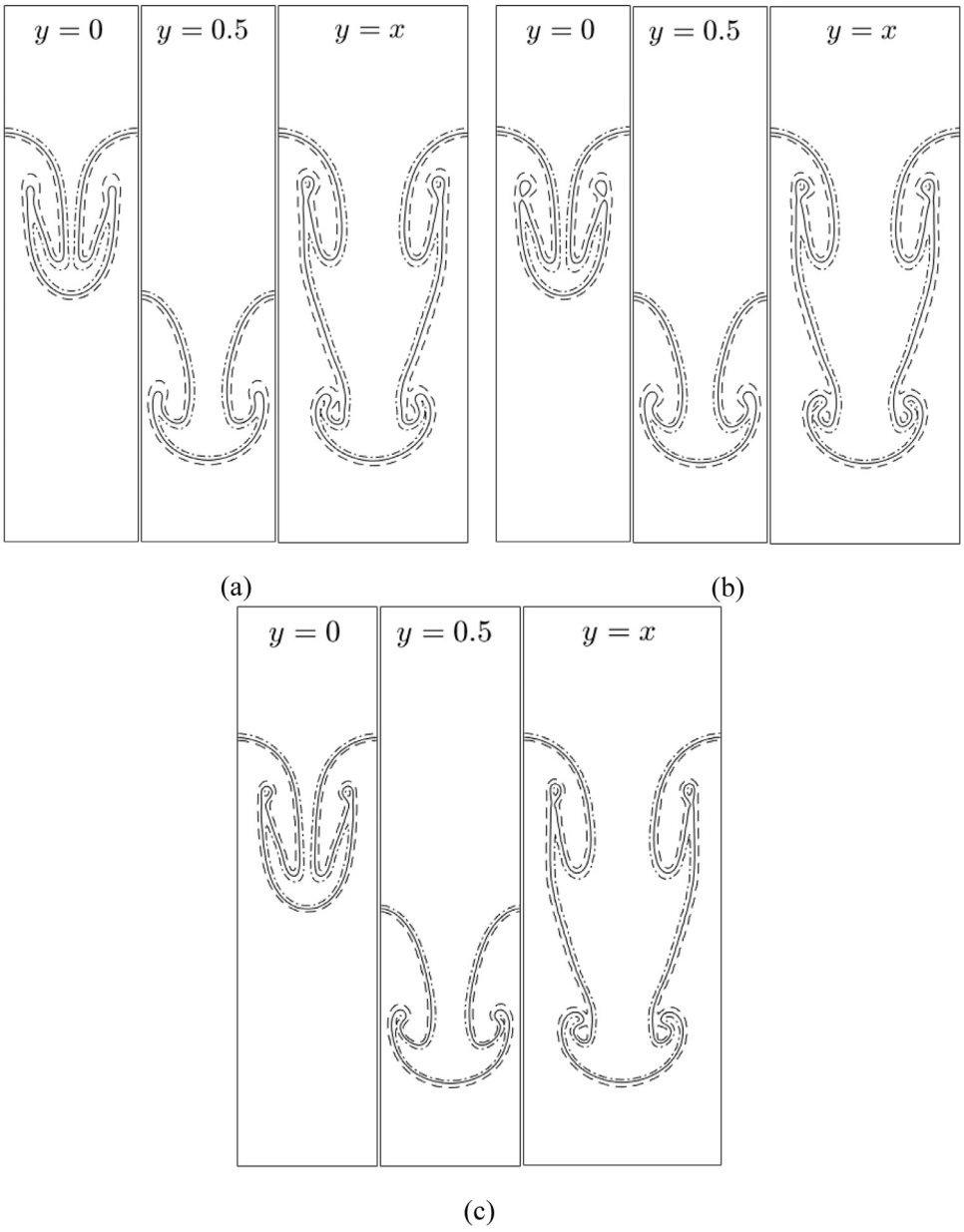

Fig. 16. Cross profiles along $y = 0$, $y = 0.5$, and $y = x$ at $t = 3$, where the dashed, solid, and dash-dotted lines represent $\phi = -0.9$, 0, and 0.9, respectively. (a) $M = 1$ and $Pe = 1/\epsilon$, (b) $M = 1$ and $Pe = 2/\epsilon$, (c) $M = \phi^2$ and $Pe = 1/\epsilon$.

3.5. Comparison with other phase-field model

We compare the proposed model with another well-known phase-field model, i.e., the conservative Allen–Cahn–Navier–Stokes (CACNS) model. As shown in previous work [37], the CACNS model can be applied to various two-phase fluid flow problems and the numerical solution of CAC model is easier than the CH model. However, the classical two-phase CACNS model is difficult to use for simulating multiple droplets system. Because of the basic dynamics of motion by mean curvature with mass conservation of the CAC model, the large droplets will grow and small droplets will shrink in time. Note that an effective way to prevent this non-physical evolution is to use the recently developed multi-phase CACNS model [38], however we only focus on the two-phase model in this research. The proposed model is derived from the two-phase CH model, thus the non-physical growth or shrink of droplets can be avoided, i.e., each droplet maintains the original mass with temporal evolution. In this test, we consider the deformations of two droplets under shear flow. The initial conditions are defined to be

$$\phi(x,y,0) = \tanh\left(\frac{0.3 - \sqrt{(x-1)^2 + (y-1)^2}}{\sqrt{2}\epsilon}\right) + \tanh\left(\frac{0.15 - \sqrt{(x-1)^2 + (y-1)^2}}{\sqrt{2}\epsilon}\right) + 1, \tag{25}$$

$$u(x,y,0) = 2y - 1, \quad v(x,y,0) = 0 \tag{26}$$

in the domain $\Omega = (0,2) \times (0,1)$. For both the CACNS model and the proposed model, we use $h = 1/64$, $\Delta t = 2h^2$, $Re = 10$, $We = 10$, $Pe = 1/\epsilon$, and $\rho_1 : \rho_2 = 1$. The gravity is ignored. Fig. 13(a) and (b) show the temporal evolutions for the CAC model and the proposed model, respectively. The temporal evolutions of local mass A enclosed by the interface for each droplet are illustrated in Fig. 14.

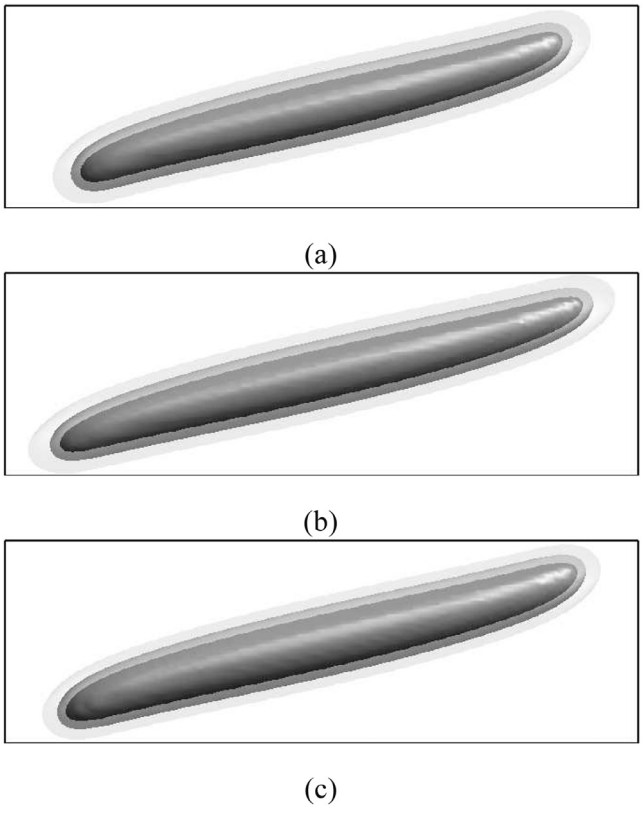

Fig. 17. Interface region at $t = 2.5$ for different models: (a) $M = 1$ and $Pe = 1/\epsilon$, (b) $M = 1$ and $Pe = 2/\epsilon$, (c) $M = \phi^2$ and $Pe = 1/\epsilon$. Here, the white gray, gray, and black gray represent the level-sets: $\phi = -0.9$, $\phi = 0$, and $\phi = 0.9$, respectively.

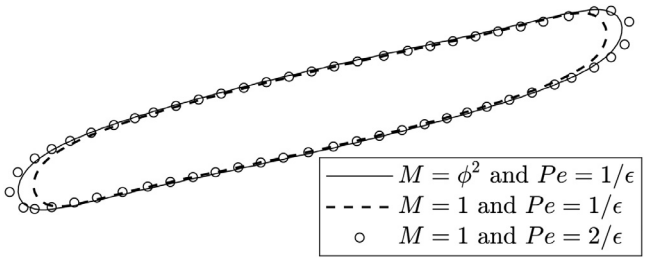

Fig. 18. Cross profiles of Interfacial positions ($\phi = 0$) at $t = 2.5$.

As we can see, the non-physical growth and shrink of droplets occur if the CACNS model is used. On the contrary, the proposed model maintains the local mass of each droplet (Fig. 18).

3.6. Three-dimensional RTI

To verify the accuracy and practicability of the proposed model in three-dimensional space, we consider the temporal evolution of three-dimensional RTI which has two-layer roll-up phenomenon and this phenomenon cannot be found in two-dimensional simulation [39]. The initial conditions are defined as:

$$\phi(x, y, z, 0) = \tanh\left(\frac{z - 2 - 0.1(\cos(2\pi x) + \cos(2\pi y))}{\sqrt{2}\epsilon}\right), \quad (27)$$

$$u(x, y, z, 0) = v(x, y, z, 0) = 0. \quad (28)$$

The following numerical parameters: $h = 1/64$, $\Delta t = 0.0025$, $Re = 3000$, $Fr = 1$, $We = \infty$, and $\rho_1 : \rho_2 = 3 : 1$ are used. The evolutions of interface ($\phi = 0$) at $t = 3$ for the classical models: $M = 1$ and $Pe = 1/\epsilon$; $M = 1$ and $Pe = 2/\epsilon$, and the proposed model: $M = \phi^2$ and $Pe = 1/\epsilon$ are shown in Fig. 15(b)–(d). Fig. 16 illustrates the cross profiles along $y = 0$, $y = 0.5$, and $y = x$ at $t = 3$ for three different models: (a) $M = 1$ and $Pe = 1/\epsilon$, (b) $M = 1$ and $Pe = 2/\epsilon$, (c) $M = \phi^2$ and $Pe = 1/\epsilon$. As we can see, the three-dimensional RTI has different evolutions along different cross views which is not found in two-dimensional simulation. For each cross profile, the proposed model not only captures the interfacial position, but also effectively keeps the interface region ($\phi = -0.9 \sim 0.9$) being uniform.

3.7. Three-dimensional drop deformation

Finally, we compare the proposed model and the classical model by considering the large deformation of three-dimensional droplet in shear flow. The initial conditions are:

$$\phi(x, y, z, 0) = \tanh\left(\frac{0.25 - \sqrt{(x-1)^2 + (y-0.5)^2 + (z-0.5)^2}}{\sqrt{2}\epsilon}\right), \quad (29)$$

$$u(x, y, z, 0) = 2z - 1, \quad v(x, y, z, 0) = 0 \quad (30)$$

in the domain $\Omega = (0, 2) \times (0, 1) \times (0, 1)$. The numerical parameters are: $h = 1/64$, $\Delta t = 2h^2$, $Re = 100$, $We = 100$, and $\rho_1 : \rho_2 = 1 : 1$. The gravity is ignored. Fig. 17(a)–(c) show the evolutions of interface region ($\phi = -0.9$: white gray, $\phi = 0$: gray, and $\phi = 0.9$: black gray) at $t = 2.5$ for three models: $M = 1$ and $Pe = 1/\epsilon$, $M = 1$ and $Pe = 2/\epsilon$, and $M = \phi^2$ and $Pe = 1/\epsilon$, respectively. The cross profiles of interface ($\phi = 0$) along $y = 0.5$ for three different models at $t = 2.5$ are illustrated in Fig. 17. In the three-dimensional case with large deformation of interface, the proposed model can also work well in capturing the interfacial position. On the contrary, the interface region is obviously relaxed or not uniform as the constant mobility is used.

Remarks. From various numerical experiments above, we can conclude that the variable mobility $M = \phi^2$ has the following two advantages: (i) The diffusion is suppressed at the center of the interfacial region where $M \approx 0$ and hence the interfacial position driven by the flow can be accurately captured without using a large value of Pe. (ii) The diffusion is only weakly suppressed away from the center of the interfacial region, and hence the interface can relax to maintain an approximately uniform thickness. In other words, the variable mobility achieves (a) an effectively large value of Pe at the center of the interfacial region to accurately capture the interfacial position and (b) an effectively small value of Pe away from the interfacial region to maintain an approximately uniform interfacial thickness.

4. Conclusions

In this article, we proposed a novel and accurate NSCH model with a nonstandard variable mobility for two-phase incompressible fluid flow. Compared to the classical mobility, the proposed phase-dependent mobility has small values nearby the interface and large values away from the interface. By minimizing the dynamics of the CH model nearby the interface, we could avoid using a large Pe number which usually caused a non-uniform interface region. Various benchmark problems, such as the RTI, droplet deformation in shear flow, and rising bubble, were performed to show that our model not only accurately capture the interfacial position, but also keep the interface region from being too much distorted. The proposed model can be easily extended to N-component ($N > 2$) fluid flows.

Declaration of Competing Interest

The authors declare that they have no known competing financial interests or personal relationships that could have appeared to influence the work reported in this paper.

CRediT authorship contribution statement

Junxiang Yang: Writing - review & editing, Software, Conceptualization, Methodology, Validation. **Junseok Kim:** Writing - original draft, Writing - review & editing, Conceptualization, Methodology, Validation.

Acknowledgments

J. Yang is supported by China Scholarship Council (201908260060). The corresponding author (J.S. Kim) was supported by Basic Science Research Program through the National Research Foundation of Korea (NRF) funded by the Ministry of Education (NRF-2019R1A2C1003053). The authors appreciate the reviewers for their constructive comments, which have improved the quality of this paper.

References

[1] Kim J. A surface tension force formulation for diffuse-interface models. J Comput Phys 2005;204:784–804.
[2] Talat N, Mavrič B, Hatić V, Bajt S, Šarler B. Phase field simulation of Rayleigh–Taylor instability with a meshless method. Eng Anal Bound Elem 2018;87:78–89.
[3] Zhang T, Wu J, Lin X. An interface-compressed diffuse interface method and its application for multiphase flows. Phys Fluids 2019;31:122102.
[4] Liang H, Shi BC, Chai ZH. Lattice Boltzmann modeling of three-phase incompressible flow. Phys Rev E 2016;93:013308.
[5] Yang J, Kim J. Phase-field simulation of Rayliegh instability on a fibre. Int J Multiph Flow 2018;105:84–90.
[6] Sahu KC, Vanka SP. A multiphase lattice Boltzmann study of buoyancy-induced mixing in a tilted channel. Comput Fluids 2011;50:199–215.
[7] Yang Q, Li BQ, Shao J, Ding Y. A phase field numerical study of 3D bubble rising in viscous fluids under an eletric field. Int J Heat Mass Transf 2014;78:820–9.
[8] Zhu CS, Han D, Xu S. Phase field simulation of single bubble behaviour under an eletric field. Chin Phys B 2018;27(9):094704.
[9] Park K, Fernandino M, Dorao CA. Numerical solution of incompressible Cahn–Hilliard and Navier–Stokes system with large density and viscosity ratio using the least-squares spectral element method. J Fluid Flow Heat Mass Transf 2016;3:73–85.
[10] Li Y, Choi JI, Kim J. A phase-field fluid modeling and computation with interfacial profile correction term. Commun Nonlinear Sci Numer Simul 2016;30:84–100.
[11] Soligo G, Roccon A, Soldati A. Mass-conservation-improved phase field methods for turbulent multiphase flow simulation. Acta Mech 2019;230:683–96.
[12] Hu Y, He Q, Li D, Li Y, Niu X. On the total mass conservation and the volume preservation in the diffuse interface method. Comput Fluids 2019;193:104291.
[13] Bai F, He X, Yang X, Zhou R, Wang C. Three-dimensional phase-field investiagtion of droplet formation in microfluidic flow focusing devices with experimental validation. Int J Multiph Flow 2017;93:130–41.
[14] Park JM, Anderson PD. A ternary model for double-emulsion formation in a capillary microfluidic device. Lab Chip 2012;12:2672–7.
[15] Zhu G., Kou J., Yao J., Li A., Sun S.. A phase-field moving contact line model with soluble surfactants. J Comput Phys. 10.1016/j.jcp.2019.109170. 2020; 405:109170.
[16] Shi Y, Tang GH, Cheng LH, Shuang HQ. An improved phase-field-based lattice Boltzmann model for droplet dynamics with soluble surfactant. Comput Fluids 2019;179(30):508–20.
[17] Nochetto RH, Salgado AJ, Tomas I. A diffuse interface model for two-phase ferrofluid flows. Comput Methods Appl Mech Eng 2016;309:497–531.
[18] Liu HR, Ding H. A diffuse-interface immersed-boundary method for two-dimensional simulation of flows with moving contact lines on curved substrates. J Comput Phys 2015;294:484–502.
[19] Zhang Q, Qian TZ, Wang XP. Phase field simulation of a droplet impacting a solid surface. Phys Fluids 2016;28:022103.
[20] Ding H, Spelt PDM, Shu C. Diffuse interface model for incompressible two-phase flows with large density ratios. J Comput Phys 2007;226:2078–95.
[21] Shen J, Yang X. Decoupled, energy stable schemes for phase-field models of two-phase incompressible flows. SIAM J Numer Anal 2015;53(1):279–96.
[22] Chen Y, Shen J. Efficient, adaptive energy stable schemes for the incompressible Cahn–Hilliard–Navier–Stokes phase-field models. J Comput Phys 2016;308:40–56.
[23] Zhu G, Chen H, Yao J, Sun S. Efficient energy-stable schemes for the hydrodynamics coupled phase-field model. Appl Math Model 2019;70:82–108.
[24] Wang Z, Dong S, Triantafyllou MS, Constantinides Y, Karniadakis GE. A stabilized phase-field method for two-phase flow at high Reynolds number and large density/viscosity ratio. J Comput Phys 2019;397:108832.
[25] Yu H, Yang X. Numerical approximations for a phase-field moving contact line model with variable densitites and viscosities. J Comput Phys 2017;334(1):665–86.
[26] Yang J, Li Y, Lee C, Kim J. Conservative Allen–Cahn equation with a nonstandard variable mobility. Acta Mech 2019. doi:10.1007/s00707-019-02548-y.
[27] Harlow FH, Welch JE. Numerical calculation of time-dependent viscous incompressible flow of fluid with free surface. Phys Fluids 1965;8(12):2182–9.
[28] Lee HG, Kim K, Kim J. On the long time simulation of Rayleigh–Taylor instability. Int J Numer Meth Eng 2011;85:1633–47.
[29] Kim J, Kang K, Lowengrub J. Conservative mutligrid methods for Cahn–Hilliard fluids. J Comput Phys 2004;193:511–43.
[30] Li Y, Choi Y, Kim J. Computationally efficient adaptive time step method for the Cahn–Hilliard equation. Comput Math Appl 2017;73:1855–64.
[31] Trottenberg U, Oosterlee C, Schüller A. Multigrid. London: Academic Press; 2001.
[32] Choi JW, Lee HG, Jeong D, Kim J. An unconditionally gradient stable numerical method for solving the Allen–Cahn equation. Phys A 2009;388:1791–803.
[33] Zu YQ, He S. Phase-field-based lattice Boltzmann model for incompressible binary fluid systems with density and viscosity contrasts. Phys Rev E 2013;87:043301.
[34] Li Q, Luo KH, Gao YJ, He YL. Additional interfacial force in lattice Boltzmann models for incompressible multiphase flows. Phys Rev E 2012;85:026704.
[35] Guermond JL, Quartapelle L. A projection FEM for varibale density incompressible flows. J Comput Phys 2000;165:167–88.
[36] Sheth KS, Pozrikidis C. Effects of inertia on the deformation of liquid drops in simple shear flow. Comput Fluids 1995;24(2):101–19.
[37] Jeong D, Kim J. Conservative Allen–Cahn–Navier–Stokes system for incompressible two-phase fluid flows. Comput Fluids 2017;156:239–46.
[38] Aihara S, Takaki T, Takada N. Multi-phase-field modeling using a conservative Allen–Cahn equation for multiphase flow. Comput Fluids 2019;178(15):141–51.
[39] Lee HG, Kim J. Numerical simulation of the three-dimensional Rayleigh–Taylor instability. Comput Math Appl 2013;66:1466–74.